

Constrained simulations of the local universe: II. The nature of the local Hubble flow

Luis A. Martinez-Vaquero¹, Gustavo Yepes¹, Yehuda Hoffman², Stefan Gottlöber³, Mira Sivan²

¹ *Grupo de Astrofísica, Universidad Autónoma de Madrid, Madrid E-280049, Spain*

² *Racah Institute of Physics, Hebrew University, Jerusalem 91904, Israel*

³ *Astrophysikalisches Institut Potsdam, An der Sternwarte 16, 14482 Potsdam, Germany*

1 September 2021

ABSTRACT

Using a suite of N-body simulations in different Cold Dark Matter (CDM) scenarios, with cosmological constant (Λ CDM) and without (OCDM, SCDM), we study the Hubble flow (σ_H) in Local Volumes (LV) around Local Group (LG) like objects found in these simulations, and compare the numerical results with the most recent observations. We show that Λ CDM and OCDM models exhibit the same behavior of σ_H . Hence, we demonstrate that the observed coldness of the Hubble flow is not likely to be a manifestation of the dark energy, contrary to previous claims. The coldness does not constitute a problem by itself but it poses a problem to the standard Λ CDM model only if the mean density within the Local Volume is greater than twice the mean matter cosmic density. The lack of blueshifted galaxies in the LV, outside of the LG can be considered as another manifestation of the coldness of the flow. Finally, we show that the main dynamical parameter that affects the coldness of the flow is the relative isolation of the LG, and the absence of nearby Milky Way like objects within a distance of about 3 Mpc.

Key words: methods: numerical – galaxies: Local Group – cosmology: dark matter

1 INTRODUCTION

The neighborhood of the Local Group (LG) is often described as being *cold*. This attribute implies that the dispersion of the radial velocities of galaxies from a pure Hubble flow is small, and the ‘smallness’ amounts to less than 100 km s^{-1} . Sandage et al. (1972) studied local departures from a uniform Hubble flow and could only put upper limits on such departures. This led Sandage et al. to conclude that $q_0 \simeq 0$ (where q_0 is the deceleration parameter). Later on Sandage & Tammann (1975) estimated that the upper limit to the mean random motion of field galaxies is $\lesssim 50 \text{ km s}^{-1}$. These early findings of Sandage, Tammann and their collaborators have been corroborated and vigorously improved by many others. Karachentsev et al. (2003) estimated the radial peculiar velocity dispersion of all galaxies within 5.5 Mpc to be 85 km s^{-1} . This value drops down to 41 km s^{-1} if members of galaxy groups are removed and distance errors are taken into account. Using a newer set of Karachentsev’s data Tikhonov & Klypin (2008) found a velocity dispersion of 97 km s^{-1} , within 7 Mpc, which reduces after correction for apex motion and distance errors only slightly to 84 km s^{-1} . Macciò et al. (2005) compiled the data

from three different sources: The Cepheid-based distance measurements of the HST Key Project (Freedman et al. 2001), distance estimates based on the surface brightness fluctuations method (Tonry et al. 2001) and Tully-Fisher distances (Tully et al. 1992). They fitted the data by $\sigma_H = 88 \pm 20 \text{ km s}^{-1} \times (R/7\text{Mpc})$, where σ_H is a measure of the dispersion of the radial velocities around a pure Hubble flow of galaxies within a sphere of radius R (a thorough discussion of the various estimates of σ_H is given below).

The observational evidences for a local cold Hubble flow seem to be indisputable. Yet, the question arises as to why a σ_H of the order of a few tens of km s^{-1} is labeled as ‘cold’. Namely, by what standard is it cold?. Rich clusters of galaxies provide the first and the most robust evidence for a departure from a pure Hubble flow, with a dispersion of peculiar velocities of up to $\approx 10^3 \text{ km s}^{-1}$. Compared with the rich clusters the neighborhood of the LG is definitely cold. A statistical estimate is also given by the pair weighted velocity dispersion (σ_{12}) which was measured from the CfA redshift survey to be $\sigma_{12}(r = 1 \text{ h}^{-1}\text{Mpc}) = 340 \pm 40 \text{ km s}^{-1}$ (Davis & Peebles 1983). Another more robust measure of the deviation from the Hubble flow is provided by the σ_1 statistics

which measures the one-dimensional rms peculiar-velocity dispersion of galaxies relative to their neighbors within a projected radius of $2 h^{-1} \text{Mpc}$ (Davis, Miller & White 1997). These authors found $\sigma_1 = 95 \pm 16 \text{ km s}^{-1}$ (for the IRAS survey) and $130 \pm 15 \text{ km s}^{-1}$ for the UGC catalog. The measured σ_1 is indeed much 'hotter' than the $\sigma_H = 25 \text{ km s}^{-1}$ within $R = 3.0 \text{ Mpc}$ (Karachentsev et al. 2009). So, with regard to the other measure of the dispersion of peculiar velocities the immediate neighborhood of the LG is indeed very cold. However, one should recall that the σ_1 and σ_{12} measures consider all galaxies in a given survey. The σ_H considered here, on the other hand, refers to one particular object, namely the LG, that resides in a dynamically quiet environment. It should be emphasized that the LG is not an atypical object, yet the LG environment is not a representative one for Milky Way like objects. This implies that, when addressing the issue of 'coldness' by means of simulations, the selection of the LG-like objects should be carefully done.

The standard model of cosmology consists of a flat Friedmann universe whose mass energy is dominated by a cosmological constant (Λ) and cold dark matter (labeled as ΛCDM). It has been recently stated that the cosmological constant, or its generalization the Dark Energy (DE), manifests itself in the dynamics of the very local universe (Baryshev et al. 2001, Chernin et al. 2004, 2007). These authors argued that the coldness of the local flow is a manifestation of the existence of the dark energy. This has been supported by Macciò et al. (2005) who analysed a set of N-body simulations and concluded that indeed "... [their] results provide new, independent evidence for the presence of dark energy on scales of a few megaparsecs". These results, if correct, would have provided an independent corroboration to the DE component whose existence is otherwise inferred from observations of distant objects and on very large scales of the Universe. The claims of Chernin et al. (2007) have been challenged by Hoffman et al. (2008), who analyzed a suit of constrained and unconstrained CDM simulations, identified LG-like objects and studied the flow field around these. The main result of Hoffman et al. (2008) invalidates the model advocated by Chernin et al. (2007) and its basic predictions. The claims made by Macciò et al. (2005) have remained unchallenged till present.

There are two main issues this paper addresses. The claim that the coldness of the local flow is induced by the dark energy, and the fact that it is strongly contradicted by Hoffman et al. (2008), motivated us to revisit the problem. Then, there is the general problem of the nature of the local flow. In particular the question of how the various characteristics of the local neighborhood are affecting the local flow is addressed here.

The present paper adopts the methodology used by Macciò et al. (2005) and later on by Hoffman et al. (2008). Namely, a set of numerical simulations is performed, ensembles of LG-like objects are constructed and σ_H is calculated around these mock objects in the same way as the Hubble flow around the actual LG is analyzed. This is further extended here. The cosmological models studied here are the presently accepted model of cosmology with a cosmological constant, ΛCDM , the open CDM (OCDM) and the outdated Einstein-De Sitter SCDM models (where S stands for the standard of the years of the 1990s and CDM stands for cold dark matter). Most of the simulations studied here

are constrained and thereby are constructed to reproduce within the simulation box the observed Large Scale Structure (LSS) on scales larger than $\approx 5 h^{-1} \text{Mpc}$. A thorough study of the nature of the local Hubble flow is done by studying the dependence of σ_H on a multitude of factors, including the cosmological parameters, the mass resolution, the very local environment and the structure on larger scales. The control over the very small scales is achieved by varying the selection rules for the LG-like objects and the control over the large scale environment is done by performing the constrained simulations. A somewhat different selection of mock objects is obtained by constraining them to have no nearby blueshifted galaxies.

The structure of the paper is as follows. A summary of the CNG data and examination of the different ways of calculating σ_H are given in §2. §3 describes the N-body simulations analyzed here and a description of the selection of the LG-like objects is presented in §4. The analysis of σ_H is conducted first along the lines of Macciò et al. (2005) (§5). Then the dependence of σ_H on the various characteristics of the LG is shown in §6 and the possible role of mass resolution, in §7. The lack of nearby blueshifted galaxies as a manifestation of the coldness of the local flow is analyzed in §8. The paper concludes with a summary and a general discussion (§9).

2 OBSERVATIONS

The Catalog of Neighboring Galaxies (Karachentsev et al. 2004, CNG) provides the latest and most comprehensive survey of the velocities of nearby galaxies. The catalog includes the distances and radial velocities of more than 400 galaxies, roughly 300 of which are in the Local Volume (LV), defined by a sphere of $R = 7 \text{ Mpc}$ about the LG. Tikhonov & Klypin (2008) have recently compiled the catalog and calculated σ_H of all the CNG galaxies within the LV. Distances are typically measured with 10% errors. Tikhonov & Klypin studied the recent, yet unpublished version of the catalog. That compilation of the data is taken here as the observational reference value, against which our numerical results are to be compared.

The local flow is studied here within the framework defined by Tikhonov & Klypin (2008). Their study ignores non-linear motions within the LG and therefore all galaxies closer than 1.0 Mpc are excluded from the analysis. The flow is analyzed by means of measuring the dispersion of the radial velocities about the Hubble flow of all galaxies found within the LV, which is redefined to correspond to the shell of $(1 - 7) \text{ Mpc}$. The choice to consider all galaxies regardless of their possible membership in galaxy groups is driven by the principle of keeping the selection to be as clear and simple as possible. This avoids the issue of defining a galaxy group catalog and simplifies the comparison of observations and simulations.

There are different ways of defining the scatter of the line-of-sight (LOS) velocities from a pure Hubble, σ_H . Consider a catalog of galaxies whose distances and radial velocities are measured, $\{(r_i, v_i)\}_{i=1, \dots, N}$. Tikhonov & Klypin (2008) estimated the apex motion of the observer, namely the LG, with respect to the sample of galaxies in the catalog and subtracted the apex velocity from the observed LOS

velocities. The dispersion σ_H is then calculated as the root mean square (RMS) with respect to the Hubble flow, where the global value of the Hubble constant (H_0) is assumed. Macciò et al. (2005) defined σ_H by the standard deviation (SDV) of the residual LOS velocities. This is equivalent to measuring the RMS of the residual velocities from the local Hubble flow, namely using the locally determined Hubble constant from the data itself (H_{loc}). Yet, a simpler approach is to associate σ_H with the RMS of the residual from the global Hubble flow. This is the approach adopted here, namely σ_H is calculated by:

$$\sigma_H^2 = \frac{1}{N} \sum_{i=1}^N [v_i - H_0 r_i]^2. \quad (1)$$

and the sum extends over the N galaxies within the appropriate distance cut of the catalog. Hereafter these methods are referred to as the APEX, SDV and RMS.

One can argue for the merits and disadvantages of the different methods and they all can be used as long as observations and simulations are analyzed consistently. Still, we argue here that the use of the dispersion around the global Hubble flow is the preferred way. The motivation for measuring σ_H stems from the information it provides on the deviations from a pure Hubble flow. By using the locally determined Hubble constant the 'breathing' (i.e. isotropic) mode of the flow is absorbed in H_{loc} , and so the resulting σ_H underestimates the actual deviation from a pure Hubble flow. In the case of the apex motion the velocity of the LG, that hosts the observer, is treated as if it is an external effect that is not related to the perturbed flow one is trying to study. It is solved in a manner which does not depend on the nature of the perturbation field. The inclusion of the apex motion of the observers provides a better measure of the deviation from a pure Hubble flow. Yet, it is shown here that the differences between the different measures are small. The different measures of σ_H have been applied to an ensemble of LG-like objects drawn from one of the high resolution simulations studied here (Λ CDMhr, see §3 for a detailed description). Figure 1 presents the results obtained for the different estimators of σ_H . The main result is that the differences between the different methods are much smaller than the scatter around the median of calculated values of σ_H .

Table 2 of Tikhonov & Klypin (2008) provides the RMS and APEX estimates of σ_H for the CNG galaxies for various radial cuts. These estimates are corrected for distance errors. The representative number used here is the RMS estimation for all galaxies within (1 – 7) Mpc of $\sigma_H = 90.4 \text{ km s}^{-1}$.

3 SIMULATIONS

A suit of constrained and unconstrained Λ CDM (flat, Λ and CDM), OCDM (open, CDM only) and SCDM (flat, CDM only) low and high resolution simulations have been performed. Table 1 lists the names and the parameters of the simulations. The five low resolution simulations ($N = 256^3$) are the same ones described in Martínez-Vaquero et al. (2007) and Hoffman et al. (2008). A computational box of $L = 64 \text{ h}^{-1} \text{ Mpc}$ (where h is Hubble's constant in units of $100 \text{ km s}^{-1} \text{ Mpc}^{-1}$) and the WMAP1 cosmological parameters are assumed for the Λ CDM simulations (Spergel et al.

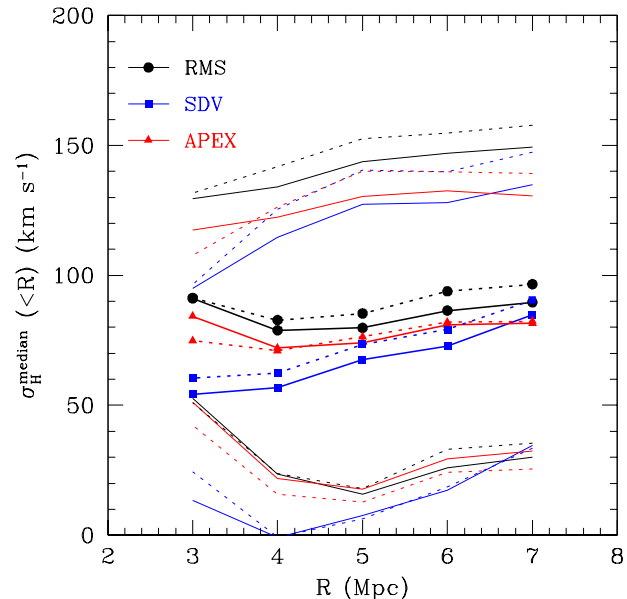


Figure 1. The median of σ_H (lines with points) and its standard deviation (thin lines) for the Λ CDMhr simulation taking all the DM halos (solid lines) and only those with a circular velocity higher than 35 km s^{-1} (dotted lines) in the distance range of (1 – R) Mpc computed using the APEX (triangles), SDV (squares) and RMS (circles) methods.

2003). The OCDM simulations are identical to the Λ CDM ones but without the Λ term, hence they correspond to an open universe. The SCDM is used here just as an extreme model for which the Hubble flow is expected to be much hotter than all other models, despite the fact that is a cosmological model which stands in marked disagreement with a wide range of cosmological observations. The five low resolution, constrained and unconstrained, simulations are all based on the same realization of the Gaussian random field. The Λ CDMhr and Λ CDM160 are high resolution ($N = 1024^3$) simulations in computational boxes of $L = 64$ and $160 \text{ h}^{-1} \text{ Mpc}$ respectively. Both are performed with the WMAP3 cosmological parameters (Spergel et al. 2007).

Five of the simulations are constrained ones, namely the initial conditions of these are set by constrained realizations of Gaussian fields. Observational data of the nearby universe is used as constraints on the initial conditions and thereby the resulting simulations reproduce the observed LSS. The basic algorithm of constraining Gaussian random fields is the one developed by Hoffman & Ribak (1991). The implementation of the algorithm to observational data and a description of the construction of constrained simulations was described at length in Kravtsov et al. (2002) and Klypin et al. (2003). A brief description of the constraining data is given here. Two different observational data is used to set up the initial conditions. The first is made of radial velocities of galaxies drawn from the MARK III (Willick et al. 1997), SBF (Tonry et al. 2001) and the Karachentsev et al. (2004) catalogs. Peculiar velocities are less affected by non-linear effects and are used as constraints as if they were linear quantities (Zaroubi et al. 1999). The other constraints are obtained from the catalog of nearby X-ray selected clusters

of galaxies (Reiprich & Böhringer 2002). Given the virial parameters of a cluster and assuming the spherical top-hat model one can derive the linear overdensity of the cluster. The estimated linear overdensity is imposed on the mass scale of the cluster as a constraint. For the CDM cosmologies the data used here constrains the simulations on scales larger than $\approx 5 h^{-1} \text{Mpc}$ (Klypin et al. 2003). It follows that the main features that characterize the local universe, such as the Local Supercluster, Virgo cluster, Coma cluster and Great attractor (in the large box), are all reproduced by the simulations. The small scale structure is hardly affected by the constraints and is essentially random.

We have used the parallel TREEPM N-body code GADGET2 (Springel 2005) to run these simulations. A uniform mesh of 512^3 grid points was used to compute the long-range gravitational force by means of the Particle-Mesh algorithm. A constant comoving Plummer equivalent gravitational smoothing scale of $20 h^{-1} \text{kpc}$ was set at high redshift and we changed it to $5 h^{-1} \text{kpc}$ physical scale since $z=3$ till $z=0$. The simulations were started at $z=50$ in all cases. We employed a variety of parallel computer architectures (SGI-ALTIX, IBM-SP4, Opteron-clusters) during the course of this work. Using 16 processors simultaneously, we completed one run in about 2 cpu days.

We analyzed also two simulations with higher mass resolution (1024^3 particles). The simulation with box size $64 h^{-1} \text{Mpc}$ has been also evolved using GADGET2. A grid of 1024^3 was used in this case for the computation of the PM forces. Gravitational smoothing was set to $1.6 h^{-1} \text{kpc}$ at high redshift and $0.8 h^{-1} \text{kpc}$ at lower redshift. The initial conditions were set up at $z = 100$ for this run. The simulation of box size $160 h^{-1} \text{Mpc}$ has been calculated by the MPI version of the Adaptive Refinement Tree (ART) code described in Gottlöber & Klypin (2008). Initial conditions were set up at $z = 30$ and the maximum number of refinement levels were set to 9, which translates into a maximum spatial resolution of $1.2 h^{-1} \text{kpc}$. These two high resolution simulations were also analyzed by Tikhonov & Klypin (2008).

We conclude this section with a general remark. The parameters of the simulations are defined by using the h^{-1} scaling. Yet, the comparison of the results with observations, and in particular the distance cuts, is made after an $H_0 = 73 \text{ km s}^{-1} \text{Mpc}^{-1}$ is assumed and distances are expressed in units of “real” Mpc.

4 SELECTION OF LG CANDIDATES

DM halos were found in simulations using two object finding methods: The Bound Density Maxima (BDM) algorithm (Klypin et al. 1999) is based on finding local center of mass in spheres of variable radius starting from randomly selected particles in the simulation. The AMIGA Halo Finder (Gill et al. 2004), on the contrary, finds local density maxima from an adaptive mesh hierarchy. In both cases, an iterative procedure to find local centre of mass from density maxima is used. Particles that are gravitationally unbound to the halo potential are also removed. Only halos with a mass higher than 2.6×10^{10} (ΛCDM , ΛCDMu , OCDM and OCDMu), 8.7×10^{10} (SCDM), 5.0×10^8 (ΛCDMhr) and $4.0 \times 10^9 M_\odot$ (ΛCDM160) are considered. For the work re-

ported here we have used the halo catalogues obtained by the AMIGA code, except for the ΛCDM160 simulation where we have used the BDM halo catalogue. In any case, we have checked that the results are independent of the halo finder.

One of the main aims of this paper is to perform a detailed comparison with Macciò et al. (2005) results, so as to be able to challenge their claim on the role of the DE in the local dynamics. In order to meet this goal the selection criteria of LG-like objects of Macciò et al. have been followed to the letter. Going beyond the comparison with that paper the selection rules are reexamined and some of which are revised. Here, these criteria are expressed in physical units without the h^{-1} scaling. The LG objects obey the following selection:

- (i) The groups contain two MW and M31 like DM halos with maximum circular velocity in the range of $125 \leq V_c \leq 270 \text{ km/s}$.
- (ii) The two major DM halos are separated by no more than 1 Mpc.
- (iii) The relative radial velocity of the two main halos is negative.
- (iv) There are no objects with maximum circular velocity higher than MW and M31 candidates within a distance of 3 Mpc.
- (v) The group resides within a distance of 7 to 17 Mpc from one and only one Virgo like halo of $500 \leq V_c \leq 1500 \text{ km/s}$. No Virgo like halos can appear within a distance of 7 Mpc.

The selected LG-like objects obeying all the above rules are defined as *Pairs*, for the fact that they are dominated by two MW and M31 like DM halos.

A careful examination of the dynamics of LG-like objects suggests the dynamics of the Hubble flow might not depend strongly on whether they are dominated by two, almost equal, massive objects or by rather one massive objects (see Macciò et al. 2005 and Tikhonov & Klypin 2008). To test this idea we construct the *Singles* ensemble of LG-like objects which obey all the criteria presented above apart from the first one. Namely, for the *Singles* objects we look for individual halos, whose mass are similar to MW and M31 together, namely $10^{12} \leq M_{\text{vir}} \leq 2 \times 10^{12} h^{-1} M_\odot$. The LV around such objects is studied.

In Table 2, the number of LG candidates found following both criteria is shown. Higher number of LG-like objects are obtained using *Singles* criterion because it is less restrictive than the *Pairs* one. One should note that there is not a one-to-one correspondence of mock LGs in the ΛCDM and OCDM simulations, even if they have the same computational box and random realization of the initial conditions. This stems for the fact that the LG constitutes a quasi-linear object, far from being in virial equilibrium. LG-like objects are delicately defined to match the observed LG and the small dynamical differences introduced by the Λ term are likely to prevent a full correspondence between objects in the different models.

Some of the simulations used here are constrained ones, namely their large scale structure is constrained to reproduce the observed cosmological neighborhood. No attempt is made here to select only LG-like objects that reside in the ‘correct’ position within the cosmic web that constitutes the local neighborhood, as this would result in a very poor statis-

MODEL	CONSTRAINED	BOX [$h^{-1}\text{Mpc}$]	Ω_m	Ω_Λ	h	σ_8	N	$m_{DM} [h^{-1}M_\odot]$
ΛCDM	yes	64	0.30	0.70	0.70	0.90	256^3	1.3×10^9
ΛCDMu	no	64	0.30	0.70	0.70	0.90	256^3	1.3×10^9
ΛCDMhr	yes	64	0.24	0.76	0.73	0.75	1024^3	1.6×10^7
ΛCDM160	yes	160	0.24	0.76	0.73	0.75	1024^3	2.5×10^8
OCDM	yes	64	0.30	0	0.70	0.90	256^3	1.3×10^9
OCDMu	no	64	0.30	0	0.70	0.90	256^3	1.3×10^9
SCDM	yes	64	1.0	0	0.50	0.7	256^3	4.4×10^9

Table 1. Description of the set-up and cosmological parameters used for the different simulations: constrained or random, computational box size, matter density (Ω_m), cosmological constant (Ω_Λ), Hubble's constant (h), initial power spectrum normalization (σ_8), number of particles (N) and mass of the DM particle (m_{DM})

Criterion	ΛCDM	ΛCDMu	ΛCDMhr	ΛCDM160	OCDM	OCDMu	SCDM
<i>Pairs</i>	13	20	12	131	11	15	24
<i>Singles</i>	52	65	43	478	38	60	78

Table 2. Number of LG candidates found in each simulation following the *Pairs* and *Singles* criteria.

tics. Rather, objects are defined as LG-like, *Pairs* or *Singles*, regardless of their location in the computational box, and the flow field around these objects is studied.

5 ANALYSIS OF HUBBLE FLOW WITHIN THE LOCAL VOLUME

The main purpose of the present section is to study the dispersion of the peculiar velocities around LG-like objects selected in the manner of Macciò et al. (2005). The flow around each object is studied using the RMS estimator of σ_H , so as to allow a comparison with the analysis of the CNG data (Tikhonov & Karachentsev 2006). The analysis consists of three parts:

- (a) The examination of the Hubble diagram of the flow around LG-like objects.
- (b) The statistical distribution of σ_H of the various models.
- (c) The dependence of σ_H on the mean density of the LV around each object.

In all cases we take a spherical shell of $(1 - 7)$ Mpc as the LV of each object and, unless otherwise stated, σ_H corresponds to all objects within the LV. Like with the actual data, the inclusion or omission of halos within 1.0 Mpc distance leaves the value of σ_H virtually unchanged.

The six panels of Fig. 2 present the combined Hubble diagram of 10 randomly chosen LG-like objects of the different models. The solid line corresponds to the unperturbed Hubble flow and the upper and lower dashed lines corresponds to $H_0 r \pm \sigma_H$, where σ_H is the median value of σ_H for each simulation. The individual points with the error bars represent the value of $\sigma_H(R)$ from Tikhonov & Klypin (2008) observational data. The results from ΛCDMhr simulation are not shown in Figures 2, 3 and 4 since they are very similar to the other ΛCDM simulations.

Table 3 presents the mean σ_H of the full LV taken over the *Pairs* and the *Singles* in each of the simulations. The fractional cumulative distribution, $\eta(\sigma_H) = N(< \sigma_H)/N_T$,

is presented in Fig. 3, where $N(< \sigma_H)$ is the number of LG-like objects colder than σ_H and N_T is the total number of LG objects. The cumulative distribution is shown for all models and for both the *Pairs* and the *Singles*. In each frame the vertical line indicates the observational value of $\sigma_H = 90.4 \text{ km s}^{-1}$ and the numbers give the fraction of LG-like objects with σ_H smaller than the observed value of the *Pairs* and the *Singles* (in parentheses).

Fig. 3 shows that there is a large scatter in the distribution of σ_H and that for all the models considered here there is a non-negligible probability to find LG-like objects with σ_H equal or smaller the one corresponding to the actual LG. However, there is another dynamical variable that controls the dynamics around these objects and that is the mean density within the LV. This was shown by Macciò et al. (2005) and it is clearly reproduced by the analysis of the models considered here. Fig. 4 shows the scatter plot of σ_H vs. the mean matter density within the LV normalized by the mean cosmological density. Both *Pairs* and *Singles* LG-like objects are studied and the results are virtually the same in the range of $\rho_{DM}/\bar{\rho}_{DM} \leq 2$, where ρ_{DM} and $\bar{\rho}_{DM}$ are the mean DM density within the LV and the cosmological mean DM density. In the simulations the DM density is very easily measured but this is not a directly observable quantity. Observationally the galaxy distribution within the LV is used to infer a local density. Short of having numerical simulations with full galaxy formation treatment the density of DM halos is used here as a proxy to the galaxy distribution. The lower panel of Fig. 4 presents the dependence of σ_H on the density of mass which belongs to halos within the LV normalized by the mean mass density of all the simulated volume. In both panels of Fig. 4 the horizontal line denotes the observational estimate of σ_H .

6 RELAXING THE LOCAL GROUP CRITERIA

The LG appears to be a very typical small group of galaxies, whose main dynamical characteristics are summarized

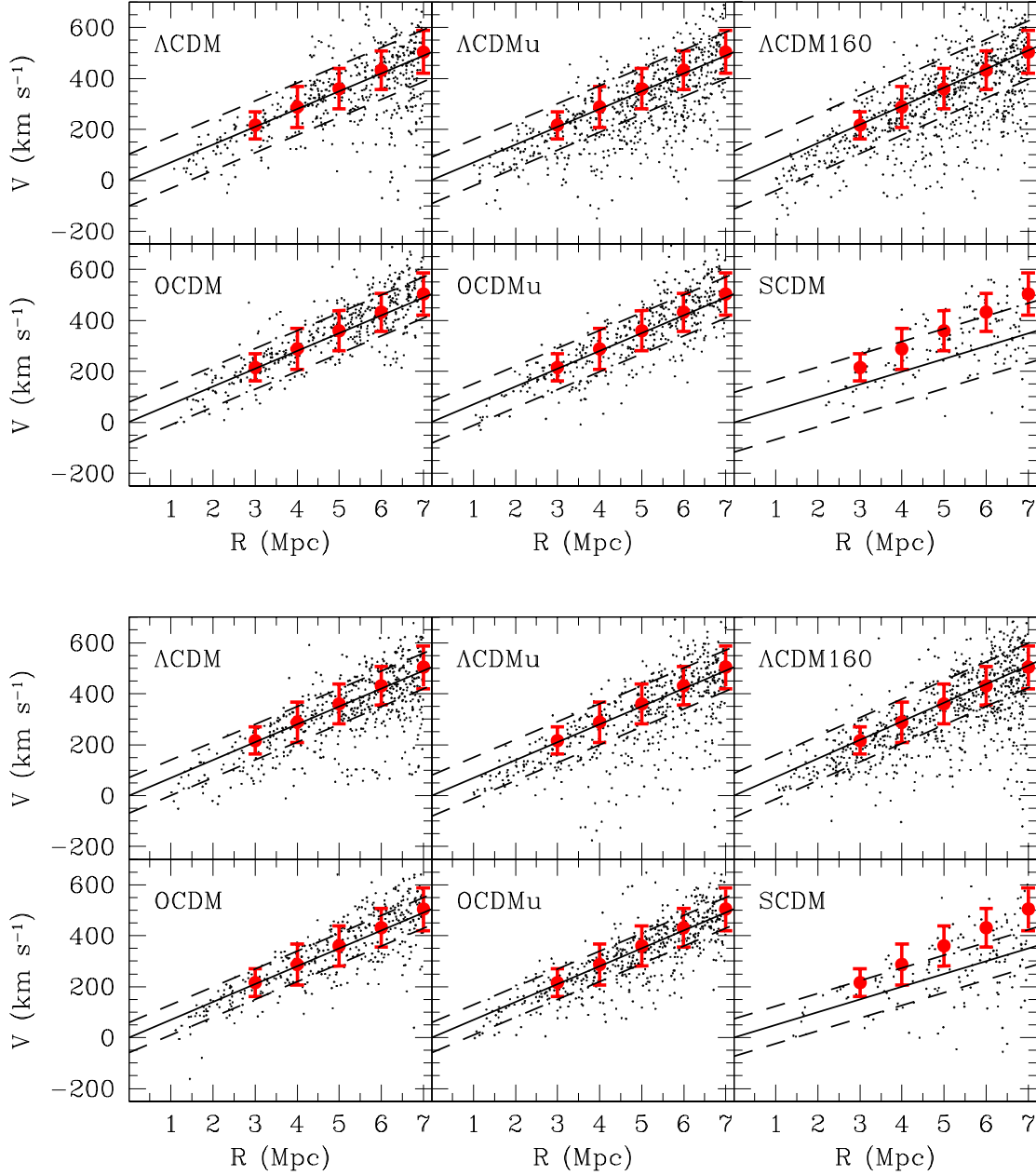


Figure 2. Combined Hubble diagrams of 10 randomly chosen LG-like objects in the different simulations. The solid lines represent the $H_0 r$ Hubble flow and the dashed ones show the median of σ_H (see Table 3). The individual data points (in red) correspond to the mean radial velocity and the σ_H dispersion in the $(1 - R)$ Mpc distance cut of the Tikhonov & Klypin (2008) data. The upper panel presents the LG-like objects selected using the *Pairs* criterion and the lower ones correspond to those LG's selected with the *Singles*.

Criterion	Λ CDM	Λ CDMu	Λ CDMhr	Λ CDM160	Ω CDM	Ω CDMu	SCDM
<i>Pairs</i>	102 ± 40	91 ± 47	90 ± 60	114 ± 58	80 ± 25	81 ± 30	117 ± 33
<i>Singles</i>	70 ± 41	80 ± 44	69 ± 42	87 ± 46	60 ± 22	60 ± 30	74 ± 38

Table 3. The median of σ_H (in km s^{-1} units) and the standard deviation from the median for all the LG candidates in each simulation selected with *Pairs* and *Singles* criteria (see Fig. 2).

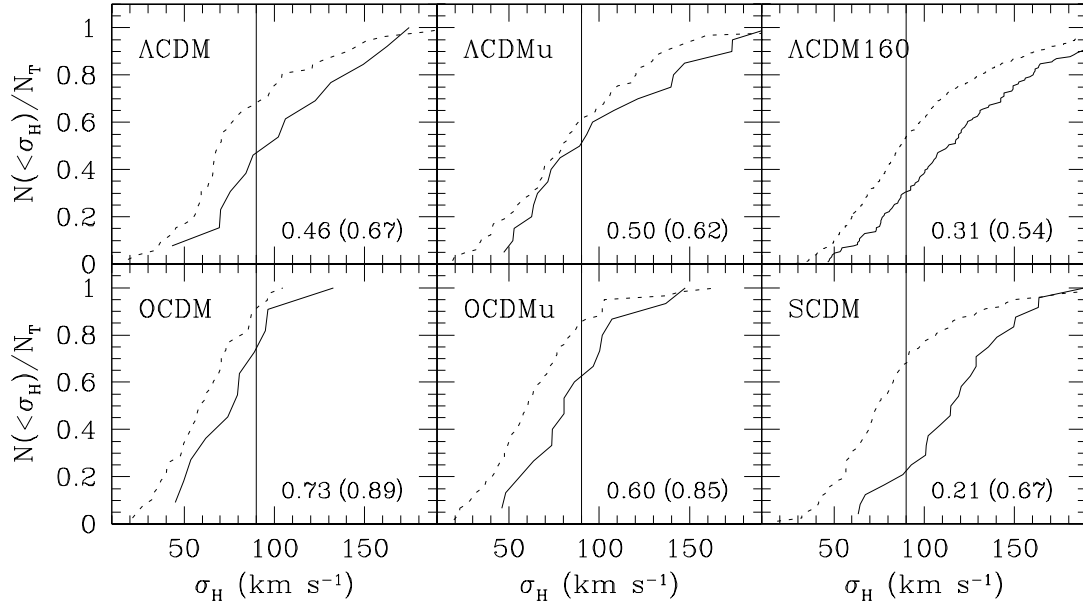


Figure 3. Cumulative number of LG candidates, from *Pairs* (solid lines) and *Singles* (dashed lines) criteria, with a σ_H lower than a given value, for the different simulations. The vertical line shows the value of the observational $\sigma_H = 90.4 \text{ km s}^{-1}$. The numbers on each frame are the fraction of LG-like objects with σ_H below this observational value for the *Pairs* and *Singles* (in parentheses).

	Distance between members (Mpc)	No neighbours (Mpc)	Virgo clusters	σ_H (km s $^{-1}$)
a	1.0	3	only one	102 ± 40
b	singles	3	only one	70 ± 41
c	1.5	3	only one	85 ± 47
d	1.0	no constrain	only one	189 ± 100
e	1.0	5	only one	104 ± 14
f	1.0	3	no constrain	113 ± 112
g	1.0	3	one or more	150 ± 74

Table 4. The median of σ_H and the standard deviation from the median for the candidates in the ΛCDM simulation for different selection criteria (see text).

in §4. These are formulated in terms of the five criteria for the selection of LG-like objects. These dynamical properties are common in the Universe, yet the particular dynamical configuration of the LG determines σ_H . It is interesting to see how these properties affect the flow field around the LG and for that purpose we have relaxed some of the criteria of §4, reselected ensembles of mock LGs and studied the cumulative histogram of σ_H for the various selections (in the ΛCDM simulation). This is shown in Table 4 and Fig. 5, where the median and the cumulative fraction of LG-like objects of the constrained ΛCDM simulation, respectively, is shown for the following cases:

- (a) The *Pairs*, which are taken as a benchmark.
- (b) The case of *Singles*.
- (c) The *Pairs* criteria, but assuming a distance between LG members lower than 1.5 Mpc.
- (d) No constraint is imposed on the lack of nearby galactic size halos.

(e) There must not be objects similar to LG members within a distance of 5 Mpc.

(f) No constraint is imposed on the existence of a Virgo-like cluster.

(g) There must be one or more Virgo-like clusters.

The *Pairs* selection is taken here as a benchmark and it is represented here for the sake of completeness. The largest departure from the benchmark *Pairs* is obtained by removing the constraint on nearby LG-like objects (case d). Table 4 and Fig. 5 clearly show the role of clusters in heating the flow. A nearby Virgo-like cluster exerts a tidal field in the vicinity of the LG-like object, resulting in a shear flow which contributes to the anisotropic component of the velocity field and thereby heating the flow. The benchmark case (a) has only one Virgo-like cluster while in case (g) there can be one or more clusters. As expected, the flow for objects found in case (g) is significantly hotter than for those found following case (a). The removal of the Virgo constraint increases somewhat the median but it more than doubles the stan-

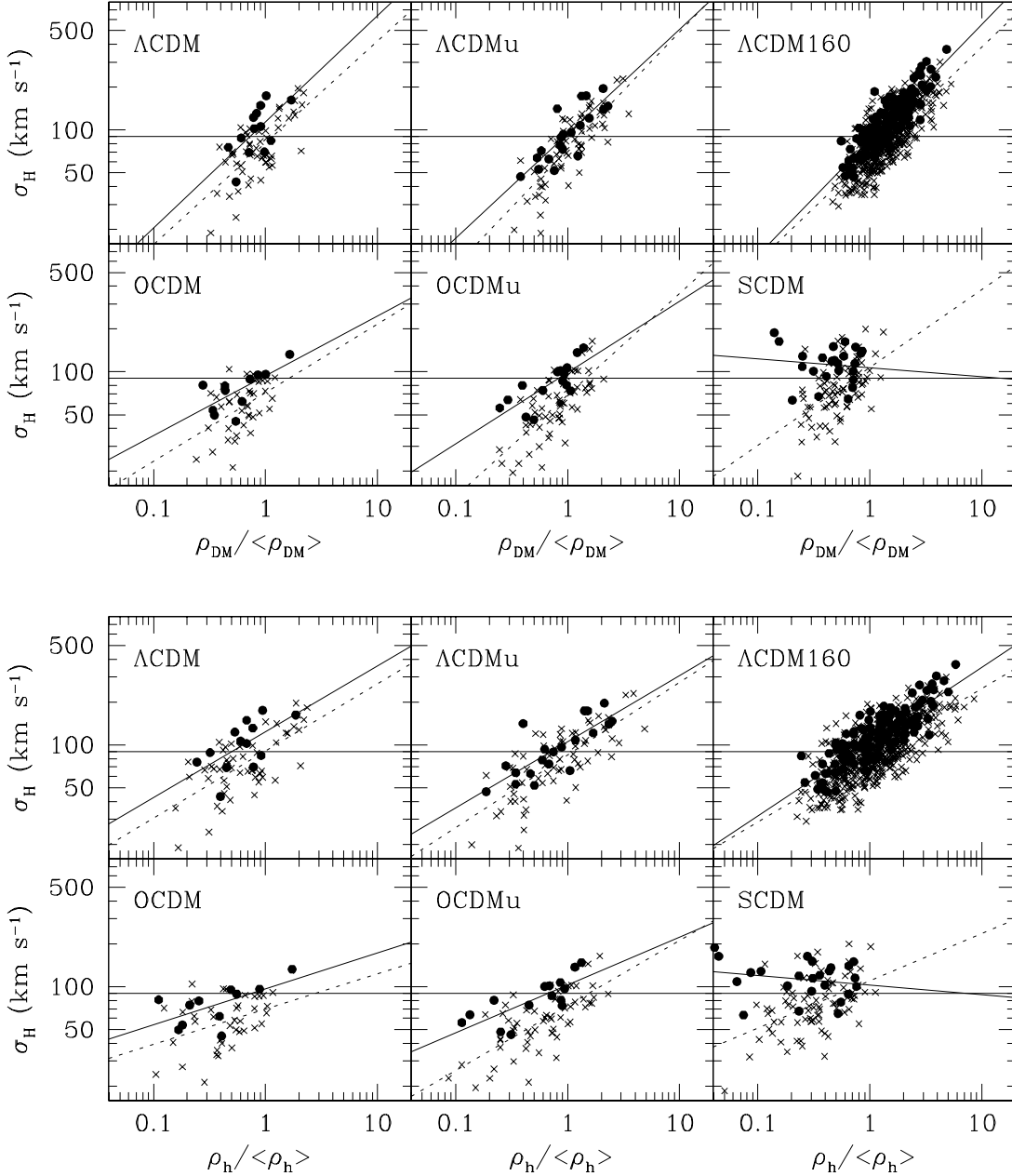


Figure 4. A scatter plot of the relation between σ_H and the mean matter density (normalized by the mean cosmological density) within the LV ($R = 7$ Mpc) for *Pairs* (solid points) and *Singles* (crosses). Power law fits to the σ_H - density scatter are shown for the *Pairs* (solid line) and *Singles* (dashed line). The horizontal line indicates the observational σ_H . In the upper panel the matter density is calculated from all DM particles inside the sphere. In the lower panel, the density is calculated from DM particles belonging to halos only.

dard deviation (case f). In such a case mock LGs can either have rich clusters within their LV, hence with very high σ_H , or can reside in low density regions far away from clusters and consequently have very low σ_H . Similarly, allowing for nearby MW size halos heats the flow and leads to many hot LG-like systems (case d). The analysis shows that the most significant selection criterium is that of the nearby halos (d). By omitting this criterion only roughly 15% of the LG-like objects have σ_H smaller than the observed value.

7 MASS RESOLUTION

The numerical simulations used here span a mass resolution that ranges over more than two orders of magnitude. The majority of the simulations are done on a very coarse grid of 256^3 and have low mass resolution. In fact, the LG-like objects of the low resolution Λ CDM and OCDM are made of about a thousand DM particles and the minimal mass of DM halos is $\approx 3 \times 10^{10} h^{-1} M_\odot$. The faint nearby galaxies

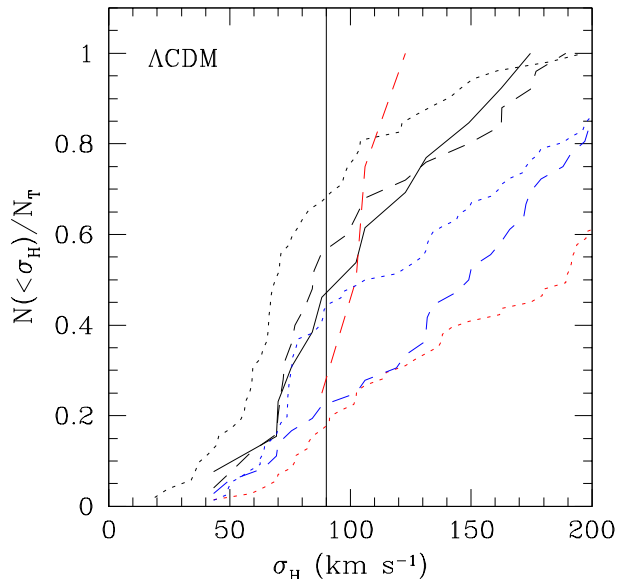


Figure 5. Fractional cumulative distribution of σ_H for the LG candidates in the Λ CDM simulation found with the different criteria shown in Table 4. The black lines correspond to *a* (solid), *b* (dotted) and *c* (dashed), the red ones to *d* (dotted) and *e* (dashed), and the blue ones to *f* (dotted) and *g* (dashed) criteria. The vertical line shows the value of the observational σ_H .

are presumably much less massive than this lower limit and the question arises as to what extent the present results are affected by the lack of resolution.

To address the issue of mass resolution we have analyzed the Λ CDMhr simulation and compared it with the Λ CDM one. This is a high resolution ($N = 1024^3$) Λ CDM (WMAP3) constrained simulation in the same $64 h^{-1}$ Mpc volume. This simulation differs from the low resolution Λ CDM one in terms of resolution, cosmological parameters and hence the power spectrum. It constitutes a different realization of the random field used to set the constrained initial conditions. An ensemble of LG-like objects has been constructed and σ_H has been calculated for all the DM halos in the corresponding LV (Figure 6, red curves) and for DM halos above the mass limit of the Λ CDM simulation ($\approx 3 \times 10^{10} h^{-1} M_\odot$; blue curves). These are compared with the cumulative distribution of the low resolution Λ CDM simulation. Figure 6 shows very clearly that, within the range studied here, the distribution of σ_H does not depend on the mass resolution.

8 THE LOCAL VOLUME AND BLUESHIFTED GALAXIES

A striking manifestation of the coldness of the local flow is the absence of blueshifted galaxies in the local neighborhood. In particular the CNG catalog shows only one blueshifted galaxy in the distance range of $(1 - 7)$ Mpc, and it is flagged as a probable member of the Virgo, i.e. its distance might be erroneous. The absence of blueshifted galaxies provides only a qualitative measure for the coldness

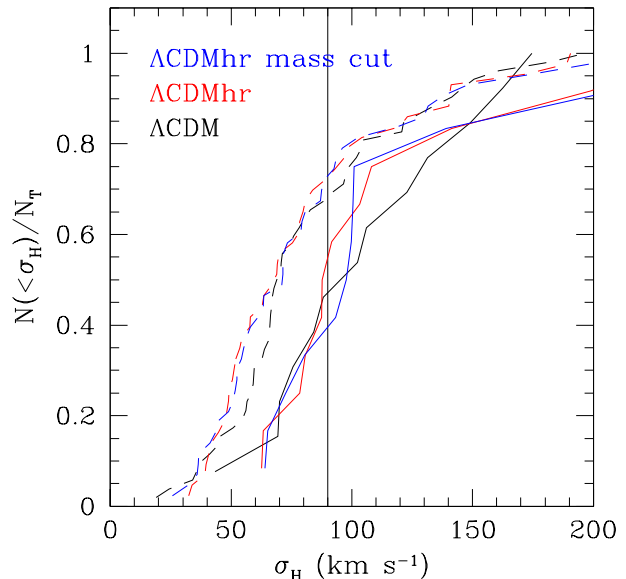


Figure 6. The fractional cumulative distribution ($\eta(\sigma_H)$), of LG candidates for simulations with different mass resolutions: The black curves correspond to the Λ CDM simulation and the red ones to the Λ CDMhr. The blue curves correspond to Λ CDMhr, but using only halos within the LG's in the same mass limit than those in the Λ CDM simulation. The solid lines correspond to the LG-like objects selected by the *Pairs* and the dashed ones to those selected by the *Singles* criteria. The vertical line shows the observational $\sigma_H = 90.4 \text{ km s}^{-1}$.

of flow, yet it constitutes a very selective criterion for finding LG-like objects (Schlegel et al. 1994). The implications of such a selection on the coldness of the flow around the selected groups are studied here.

A word of caution is due before applying the constraint of no blueshifted 'galaxies' to the LG-like objects. Here, the local velocity field is traced by DM halos. It follows that the number of blueshifted objects might depend on the mass resolution of the simulations. We follow here Tikhonov & Klypin (2008) and assume that in the Λ CDM model DM halos with $V_{\text{circ}} > 35 \text{ km s}^{-1}$ serve as proxy for observed luminous galaxies in the LV. Such halos are well resolved in the two high resolution simulations to which the no blueshifted 'galaxies' selection is applied. Table 5 lists the results of σ_H analysis applied to the Λ CDMhr and Λ CDM160 simulations. The analysis is applied to DM halos with $V_{\text{circ}} > 35 \text{ km s}^{-1}$. The analysis is applied to all the LG-like objects and then to groups that contain no blueshifted galaxies in the shell corresponding to $(x - 7)$ Mpc, where $x = 2, 3$ and 5 Mpc. The Table lists the number of LG-like objects and the median and standard deviation of σ_H of the selected objects. Figure 7 shows the cumulative histogram of σ_H for the Λ CDMhr and Λ CDM160 simulations. The figure presents the benchmark case of all pairs and the objects with no blueshifted $V_{\text{circ}} > 35 \text{ km s}^{-1}$ DM halos in the $5 - 7$ Mpc and $3 - 7$ Mpc shells. Figure 8 shows a scatter plot of σ_H against the mean density within the LV, for the same objects considered in Figure 7.

As expected, both Table 5 and Figure 7 show that the

constraint of no having blueshifted galaxies implies LG-like objects with cold environments. Both high-resolution simulations have yielded objects with no blueshifted galaxies. As can be deduced from Table 5, the closer to the LG we look for blueshifted galaxies, the less number of LG's pass the criterion. Given the uncertainties involved in the association of $V_{circ} \gtrsim 35 \text{ km s}^{-1}$ halos with nearby faint galaxies, we think that the number of LG-like objects with no blueshifted galaxies cannot be used as a reliable statistic of the local environment. Yet, it provides another strong observational evidence for the coldness of the local flow. Figure 8 provides further support to our earlier findings about the relation between σ_H and the mean density of the LV (Figure 4). LG-like objects with no blueshifted 'galaxies' in their LV are cold, $\sigma_H \lesssim 100 \text{ km s}^{-1}$, and they resides in LV with $\rho_{DM}/\bar{\rho}_{DM} \lesssim 2$.

9 DISCUSSION

A suite of CDM simulations have been used to study the nature of the velocity field around Local Group - like objects. The objects are selected so as to reproduce the main dynamical properties of the LG, which include the range of masses of the two most massive DM halos in the group, the proximity to a Virgo-like cluster and the absence of nearby massive halos. The flow field has been analyzed by means of σ_H , which is defined by the RMS value of the residual from the pure Hubble flow, of all galaxies within the Local Volume, defined to be the volume enclosed within a radius of 7 Mpc around the LG. The results are compared with the σ_H calculated for the CNG data. Two important conclusions are reached here. The first, and the more important one, is that there is no 'coldness of the local flow' problem, but rather it is the relation between σ_H and the mean local matter density that needs to be addressed in the context of the LV. The other is that within the canonical CDM cosmological models σ_H depends only on the mean matter density and not on the cosmological constant. Recently, Tikhonov et al. (2009) have found a similar cold flow around LG-like objects in a model with Warm Dark Matter (WDM) of 1 keV particle masses which leads to a cut-off in the power spectrum above $k_{peak} = 3.7 \text{ h}^{-1} \text{ Mpc}$.

The main result that has been found is that for all models considered here there is a non-negligible fraction of the LG-like objects with σ_H close to the observed value. The two Λ CDM simulations in the box $64 \text{ h}^{-1} \text{ Mpc}$ have about (30 – 45)%, the Λ CDM160 has 25%, the two OCDM simulations have roughly (50 – 65)% and even the SCDM model has 17%, of their (*Pairs*) LG-like objects colder than the observed value. However the scatter in σ_H is not random but it correlates strongly with the mean matter density within the LV, with higher σ_H expected for higher density. In the canonical Λ CDM case a $\sigma_H \lesssim 100 \text{ km s}^{-1}$ implies that the mean LV density is less than twice mean cosmological density. This is also consistent with the requirement that there are no blueshifted galaxies in the LV around the LG. It follows that the old 'coldness of local flow' problem reappears as a potentially new problem, namely the local density - coldness relation. The recent compilation of the abundance of galaxies in the LV of Tikhonov & Klypin (2008) provides interesting results. These authors studied the lu-

minosity function of the galaxies in the CNG data and estimated the LV fractional density to be about 1.4 ± 0.17 within $R = 8 \text{ Mpc}$. Using DM halos with $V_{circ} > 35 \text{ km s}^{-1}$ as a proxy to luminous galaxies, the Λ CDM predicted density enhancement in the LV stands in good agreement with the observed value. The realization that σ_H and the local density are closely connected provides another reminder to the fact that progress in understanding the local dynamics depends on a parallel advance in understanding galaxy formation.

It has been speculated that the coldness of the local flow is a manifestation of the dark energy, which dominates the mass-energy density of the universe (Baryshev et al. 2001, Chernin et al. 2004, 2007, Macciò et al. 2005). The basic argumentation behind that claim is that very locally the gravitational field is supposed to be dominated by the cosmological constant and hence the induced Hubble flow is expected to be cold. This claim has been refuted by Hoffman et al. (2008) who showed that within a local volume defined by $0.75 \leq R \leq 2 \text{ Mpc}$ the flow is dominated by the DM, regardless of the existence of a cosmological constant. Namely, the OCDM and Λ CDM models yield virtually the same σ_H within that volume. The current paper extends the numerical experiments and reinforces the results of Hoffman et al. (2008). That earlier work is extended to cover more simulations of higher resolution and the LV is defined to extend over $1 \leq R \leq 7 \text{ Mpc}$.

The current work substantiate and gives justification to the theoretical arguments suggested by Hoffman et al. (2008) as to why dark energy does not dictates the local dynamics. The arguments on the role of the dark energy are all based on approximating the local dynamics by the monopole term, i.e. a gravitational field induced by an isolated point-like object. This would have implied a very tight correlation between σ_H and the mean overdensity within the LV, contrary to the large scatter manifested by Figure 7. The arguments advocating the cooling of the local flow by the dark energy completely ignore the environmental effects on the flow. These effects are very clearly demonstrated in Table 4 which shows that σ_H nearly doubles by removing from the benchmark criteria the constraint on the lack of MW-like halos within a sphere of 3 Mpc. The proximity of Virgo-like halos also changes the value of σ_H . It follows that the dynamics of quasi-linear objects such as the LG cannot be properly modeled without a detailed accounting of environmental effects.

The present paper reaches radically different conclusions than those expressed in Macciò et al. (2005) concerning the role of the cosmological constant in shaping the dynamics of the LV. Yet, a close inspection shows that there is no technical disagreement between the two papers. We were careful to follow the selection criteria of LG-like objects of Macciò et al. (2005) and hence their Λ CDM simulation can be directly compared with the present ones. In spite of the somewhat different value of the physical parameters of the Λ CDM model used in the two papers the scatter of σ_H and its dependence of the local density are in close agreement. A careful reading of Macciò et al. (2005) reveals that their statement concerning the role of the Λ term is based on the comparison these authors did with the OCDM simulation of Governato et al. (1997).

A careful comparison with the $\sigma_H - \delta\rho/\rho$ relation of

no negative velocity halos	Λ CDMhr		Λ CDM160	
	LG candidates	σ_H^{median}	LG candidates	σ_H^{median}
all	12	97 ± 61	131	115 ± 58
5-7 Mpc	7	85 ± 15	46	90 ± 31
3-7 Mpc	4	85 ± 16	15	95 ± 31
2-7 Mpc	1	$69 \pm -$	6	99 ± 19

Table 5. The case of LG-like objects with no blueshifted galaxies: The left column presents the selection criteria of the LG-like objects: all - the benchmark *Pairs*, the following rows corresponds to LG-like objects with no blueshifted DM halos with $V_{circ} > 35 \text{ km s}^{-1}$, taken as a proxy to observed galaxies, within the respective shell. Each row provides the number of such groups and the median of σ_H and its standard deviation measured within their LV. The analysis was applied to the two high resolution simulations, Λ CDMhr and Λ CDM160.

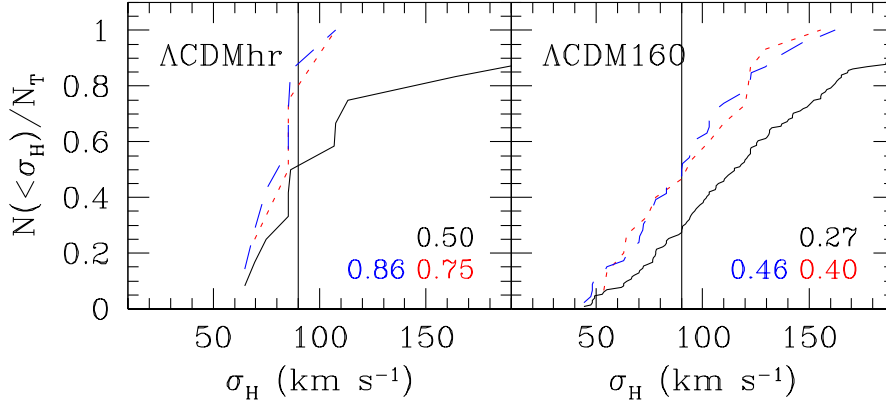


Figure 7. The Fractional cumulative distribution of LG candidates ($\eta(\sigma_H)$) for the two high resolution Λ CDMhr (left) and Λ CDM160 (right) simulations. the solid line corresponds to the *Pairs* criterion, the other two lines represents groups with no blueshifted DM halos with $V_{circ} > 35 \text{ km s}^{-1}$ within 5 – 7 Mpc (red-dotted) and 3 – 7 Mpc (blue-dashed) shells. The vertical line shows the observational $\sigma_H = 90.4 \text{ km s}^{-1}$.

the LG candidates in the OCDM simulation shown in Fig. 11 of Governato et al. (1997), and its presentation in Fig. 2 of Macciò et al. 2005, reveals that it can be reproduced in the present OCDM simulations by omitting the Virgo constraints on the selection of the LG-like objects. Given the present much better resolution, the number of our LG candidates is considerable larger than in Governato et al. (1997), in particular in the densest environments. The linear fit shown in Fig. 11 of Governato et al. is biased towards the LGs located in $\delta\rho/\rho \leq 1$, where most of their LGs are found. Restricting our fit to LGs with $\delta\rho/\rho \leq 1$, a quite similar fit emerges. This indicates that the old and present OCDM simulations equally reproduce, to within their resolution limits, the same kind of LG candidates. To summarize, by neglecting the Virgo constraints on the selection of LG-like objects and by restricting the analysis to less dense objects the old OCDM results are recovered. This might hint that the OCDM σ_H analysis of Governato et al. (1997) was performed with respect to their ‘cat2’ catalog rather than the stated ‘cat3’ catalog, in which the Virgo constraints were imposed.

No substantial differences are found between the constrained and unconstrained simulations. The constraints imposed here are affecting the structure on scales larger than $\approx 5 \text{ h}^{-1} \text{ Mpc}$ (Klypin et al. 2003), a scale that coincides with the LV. This implies that the behavior of σ_H predominantly

depends on the internal dynamics within the LV and less on the one induced by larger scales. This also gives further support to the claim that, apart from the particularities of the very nearby structure, the universe around us constitutes a very typical realization of the CDM cosmogonies. The particular dynamical attributes of the LG are its mass range of about $10^{12} \text{ h}^{-1} \text{ M}_\odot$, its binary nature, the proximity to the Virgo cluster and the absence of similar nearby objects. These have been used as the selection criteria of LG-like objects in the simulations. In §6 these criteria have been relaxed, while keeping the mass to be roughly the LG mass. One expects that the proximity of the Virgo cluster heats the flow field in the vicinity of the LG, due to its tidal field which induces non-isotropic motions around the LG. Hence the relaxation of the condition for a nearby Virgo-like cluster leads to colder LG-like objects. Similarly, in LG-like objects with a single MW-like halo the gravitational field is dominated by a monopole term and this leads to a colder flow than in binary LG-like systems. On the other hand the largest, yet opposite, effect is introduced by allowing MW-like halos to be close to the LG. The presence of such nearby halos heats the flow considerably. It follows that the main ingredient that is responsible for the coldness of the local flow is the relative isolation, and therefore also the low mean local density, of the LG. Furthermore, in the CDM cosmologies the coldness of the local flow depends more on the properties

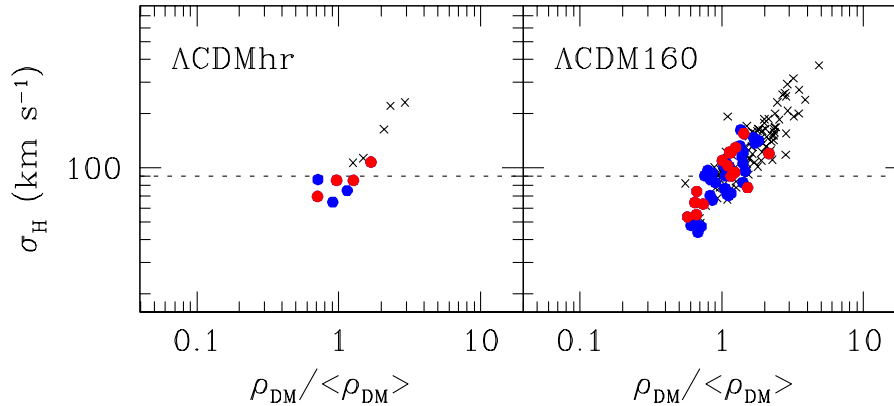


Figure 8. Scatter plots of σ_H vs. the mean matter density, normalized by the mean cosmological density, within the LV's found in the high resolution simulations, Λ CDMhr (left) and Λ CDM160 (right). All symbols correspond to LV's around LG-like objects found with the *Pairs* criterion in both simulations. The filled circles represent LV's with no blueshifted DM halos with $V_{circ} > 35 \text{ km s}^{-1}$ within the 5 – 7 Mpc shell (blue) and within 3 – 7 Mpc shell (red). The crosses are for the rest of the LV's.

of the LG than on the possible presence of a dark energy component.

10 ACKNOWLEDGEMENTS

Fruitful discussions and correspondence with I. D. Karachentsev, A. Klypin, A. Maccio and A. Tikhonov are gratefully acknowledged. This research has been supported by the ISF (13/08 at the HU). The support of the European Science Foundation through the ASTROSIM Exchange Visits Program is acknowledged (SG, YH). The simulations were performed and analyzed on the Leibniz Rechenzentrum Munich (LRZ), the Barcelona Supercomputing Center (BSC) and the Magerit supercomputer at the Centro de Supercomputación y Visualización de Madrid (CeSViMa). SG acknowledges a Schonbrunn Fellowship at the Hebrew University Jerusalem. GY would like to thank also MEC (Spain) for financial support under project numbers FPA2006-01105 and AYA2006-15492-C03. LAMV acknowledges financial support from Comunidad de Madrid through a PhD fellowship.

REFERENCES

- Baryshev Y. V., Chernin A. D., Teerikorpi P., 2001, *A&A*, 378, 729
- Chernin, A. D., Karachentsev, I. D., Teerikorpi, P., Valtonen, M. J., Byrd, G. G., Efremov, Y. N., Dolgachev, V. P., Domozhilova, L. M., Makarov, D. I., & Baryshev, Y. V. 2007, *ArXiv e-prints*, 0706.4068
- Chernin, A. D., Karachentsev, I. D., Valtonen, M. J., Dolgachev, V. P., Domozhilova, L. M., & Makarov, D. I. 2004, *A&A*, 415, 19
- Davis M., Peebles P. J. E., 1983, *ApJ*, 267, 465
- Freedman W. L., Madore B. F., Gibson B. K., Ferrarese L., Kelson D. D., Sakai S., Mould J. R., Kennicutt Jr. R. C., Ford H. C., Graham J. A., Huchra J. P., Hughes S. M. G., Illingworth G. D., Macri L. M., Stetson P. B., 2001, *ApJ*, 553, 47
- Gill S. P. D., Knebe A., Gibson B. K., 2004, *MNRAS*, 351, 399
- Gottlöber S., Klypin A., 2008, in Wagner, S. and Steinmetz, M. and Bode, A. and Brehm, M. ed., *High Performance Computing in Science and Engineering, The ART of Cosmological Simulations*. Springer-Verlag, p. 29
- Governato F., Moore B., Cen R., Stadel J., Lake G., Quinn T., 1997, *New Astronomy*, 2, 91
- Hoffman Y., Martinez-Vaquero L. A., Yepes G., Gottlöber S., 2008, *MNRAS*, 386, 390
- Karachentsev I. D., Karachentseva V. E., Huchtmeier W. K., Makarov D. I., 2004, *AJ*, 127, 2031
- Karachentsev I. D., Makarov D. I., Sharina M. E., Dolphin A. E., Grebel E. K., Geisler D., Guhathakurta P., Hodge P. W., Karachentseva V. E., Sarajedini A., Seitzer P., 2003, *A&A*, 398, 479
- Karachentsev I. D., Kashibadze O. G., Makarov D. I., Tully R. B., 2009, *MNRAS*, 393, 1265
- Klypin A., Gottlöber S., Kravtsov A. V., Khokhlov A. M., 1999, *ApJ*, 516, 530
- Klypin A., Hoffman Y., Kravtsov A. V., Gottlöber S., 2003, *ApJ*, 596, 19
- Kravtsov A. V., Klypin A., Hoffman Y., 2002, *ApJ*, 571, 563
- Macciò A. V., Governato F., Horellou C., 2005, *MNRAS*, 359, 941
- Martinez-Vaquero L. A., Yepes G., Hoffman Y., 2007, *MNRAS*, 378, 1601
- Reiprich T. H., Böhringer H., 2002, *ApJ*, 567, 716
- Sandage A., Tammann G. A., 1975, *ApJ*, 196, 313
- Sandage A., Tammann G. A., Hardy E., 1972, *ApJ*, 172, 253
- Schlegel D., Davis M., Summers F., Holtzman J. A., 1994, *ApJ*, 427, 527
- Spergel, D. N., et al. 2007, *ApJS*, 170, 377
- Spergel, D. N., et al. 2003, *ApJS*, 148, 175
- Springel V., 2005, *MNRAS*, 364, 1105
- Tikhonov A., Karachentsev I. D., 2006, *ApJ*, 653, 969
- Tikhonov A., Klypin A., 2008, *ArXiv e-prints*, 0807.0924
- Tikhonov, A. V., Gottlöber, S., Yepes, G., Hoffman, Y., in preparation, (2009)

- Tonry J. L., Dressler A., Blakeslee J. P., Ajhar E. A.,
Fletcher A. B., Luppino G. A., Metzger M. R., Moore
C. B., 2001, *ApJ*, 546, 681
Tully R. B., Shaya E. J., Pierce M. J., 1992, *ApJS*, 80, 479
Willick J. A., Courteau S., Faber S. M., Burstein D., Dekel
A., Strauss M. A., 1997, *ApJ*, 109, 333
Zaroubi S., Hoffman Y., Dekel A., 1999, *ApJ*, 520, 413